

Organofunctionalized Nb₂O₅ Nanoparticles for Photodynamic Therapy against A549 Cancer Cells

Ronaldo C. S. Oliveira,^a Luiz Henrique C. dos Santos,^{a,b} Zeinab Ghasemishahrestani,^a Marcos D. Pereira,^a Josué Sebastián B. Forero,^a Grazieli Simões,^a Emerson S. Ribeiro[✉]*,^{a,b} and Rodrigo José Corrêa[✉]*,^{a,b}

^aInstituto de Química, Universidade Federal do Rio de Janeiro (UFRJ), CT, Bloco A, Cidade Universitária, Ilha do Fundão, 21941-909 Rio de Janeiro-RJ, Brazil

^bInstituto de Química, Instituto Nacional de Tecnologias Alternativas para Detecção, Avaliação Toxicológica e Remoção de Micropoluentes e Radioativos (INCT-DATREM), Universidade Estadual Paulista (Unesp), CP 355, 14800-900 Araraquara-SP, Brazil

Niobium pentoxide shows an interesting reactivity that allows the control of different aspects of its morphology and chemistry. In this study, Nb₂O₅ nanoparticles were modified with protoporphyrin IX (PPIX) and tris(ethynylphenyl) pyrene derivative (PyPh₃) by using 3-aminopropyltriethoxysilane as linkage group and used as photosensitizers against lung cancer. The antitumor photoactivity against the A549 tumor cell line as a model of *in vitro* study showed half maximal inhibitory concentration (IC₅₀) ca. 15 μmol L⁻¹ for both materials and the absence of dark activity, indicating the viability of dye-modified Nb₂O₅ as a photodynamic therapy (PDT) agent.

Keywords: nanoparticle, niobium pentoxide, dye, photoactivity, cancer cell

Introduction

Recently, the human population in the world reached 8 billion people. This number poses new challenges in public health, food production, energy demand, sustainability, etc. Public health is particularly problematic in an overpopulation scenario and is a serious problem for governments, as its roots impact various sectors of society and consume unprecedented amounts of resources. Among the huge diversity of public health problems, cancer remains the number one cause of death, reaching 13% of all deaths,¹ despite research advances in the last decades, where lung, prostate, and breast cancer are among the most common types. In such a hostile scenario, it is necessary to develop new therapeutical strategies to expand the coping arsenal of the medicine.

Photodynamic therapy (PDT) is currently being seen as a potential procedure to treat malignant diseases.^{2,3} The main idea of this alternative therapy involves the use of photosensitizers activated by an appropriate light.⁴ Once in the target tissue, the photosensitizer (PS) can be excited by the light, triggering two main biomolecule oxidation

mechanisms, named Type I and Type II.^{5,6} Type I occurs by direct interaction of the electronically excited PS with biomolecules, where electron or hydrogen atoms are transferred between participants. In contrast, in the Type II mechanism, the electronically excited PS transfers its energy to dissolved triplet oxygen, forming the electrophilic singlet oxygen species.⁷ On both mechanisms, the generation of oxidant reactive oxygen species (ROS) will promote the oxidation of biomolecules like membranes, proteins, lipids, and even nucleic acids, leading to cell death.

Historically, PDT was initiated by employing solely the PS directly onto diseased cells. The following step was achieved by developing molecules with high light absorption capacity. Although a promising therapeutic approach, PDT showed relevant drawbacks due to PS toxicity and solubility.⁸ Thus, recently, PS-loaded nanomaterials have been studied as a direct demand for increasing PDT efficiency. Among the various possible ways to increase PDT usage relies on minimizing PS toxicity and improving cell uptake.⁸ Both cases have been evaluated by attaching the PS on the surface of different nanomaterial supports like silica, TiO₂, graphene oxide, graphene quantum dots, etc.⁸⁻¹⁵

Niobium pentoxide is a promising material for PDT due to its unique acid surface combined with the possibility

*e-mail: emersonsr@iq.ufrj.br; rodrigojosecorrea@gmail.com

Editor handled this article: Célia M. Ronconi (Associate)



of controlling its morphology, porous structure, and crystallinity.¹⁶⁻¹⁸ Further, several interesting properties such as light absorption, band gap ranging from 3.1 to 4.0 eV,¹⁹ and high adsorption capacity indicate the potential application of this material in different areas. In this study, Nb₂O₅ nanoparticles were functionalized with protoporphyrin IX (PPIX) and tris(ethynylphenyl) pyrene derivative (PyPh₃) by using 3-aminopropyltriethoxysilane as linkage group. Finally, the phototoxicity of these materials was evaluated under visible light irradiation using the lung cancer cell line A549 as a prototype test.

Experimental

Protoporphyrin IX and NbCl₅ were purchased from Sigma-Aldrich (São Paulo, SP, Brazil) and used as received. PyPh₃ was synthesized according to the literature procedure through Sonogashira reaction.²⁰ Unless specifically noted, all solvents used were high performance liquid chromatography (HPLC, Tedia, Fairfield, OH, USA) grade and checked for fluorescent impurities.

Synthesis of Nb₂O₅ nanoparticles (Nb₂O₅NP)

Nb₂O₅ nanoparticles were synthesized according to the reported literature procedure.²¹ Briefly: a mixture of NbCl₅ (1 g) in ethanol (2 mL) was added to 40 mL of aqueous solution NH₄OH (0.3 mol L⁻¹), and the mixture was stirred at 25 °C for 4 h. Afterward, the white solid formed, hydrated amorphous niobium pentoxide (Nb₂O₅.nH₂O, niobic acid), was separated from the solution by centrifugation. The solid was washed with distilled water and then centrifuged five times to remove impurities. After, in a Schlenk tube, the niobic acid was dispersed in 4 mL of hydrogen peroxide solution (30%), and the mixture was cooled with ice and stirred for 5 min, forming a colloidal dispersion of niobic acid. The colloidal dispersion was then heated at 75 °C for one week under an argon atmosphere, and finally, the product was dried for 10 h at 75 °C.

Organic functionalization of Nb₂O₅ nanoparticles with 3-(2-aminoethyl amino)propyl]trimethoxysilane

To 1 g of Nb₂O₅ nanoparticles suspended in dried toluene (100 mL) was added 15 mL of 3-aminopropyltriethoxysilane (APTES).²² The reaction was maintained at 100 °C for 24 h under constant stirring in an argon atmosphere. The resulting amino-functionalized Nb₂O₅ (Nb₂O₅NP-APS) was thoroughly washed in a Soxhlet extractor for 6 h with ethanol and then dried at 60 °C in oven under vacuum (10⁻³ mm of Hg) for 4 h.

Amidation of Nb₂O₅NP-APS with organic dyes

First, PPIX (1 mmol; 0.562 g) and PyPh₃ (1 mmol; 0.588 g) were converted into their respective acyl chloride by refluxing the dyes with thionyl chloride (68 mmol; 8.01 g) for 2 h in an argon atmosphere. Excess thionyl chloride was removed by evaporation under reduced pressure. Then, 0.46 g of Nb₂O₅NP-APS was added to a solution of each dye in anhydrous chloroform (20 mL). The resulting mixture was refluxed for 5 h and stirred overnight at room temperature. The prepared materials were washed with chloroform (5 mL) and centrifuged at 6000 rpm for 5 min until UV-Vis detected no dye in the chloroform phase.²¹ The resulting materials were named Nb₂O₅NP-APS-PPIX and Nb₂O₅NP-APS-PyPh₃.

Characterization of nanomaterials

Scanning electron micrographs (SEM) for Nb₂O₅NP and Nb₂O₅NP-APS were obtained after dispersing the samples on double-sided conductive tape on gold support. SEM images were acquired using a Jeol model JSM 6460LV scanning electron microscope at an acceleration voltage of 30.0 kV (Tokyo, Japan) and 30,000× magnification. Transmission electronic micrographs (TEM) for Nb₂O₅NP-APS-PPIX and Nb₂O₅NP-APS-PyPh₃ samples were acquired by dispersing the samples in water, and then drying them at room temperature and analyzed with a Tecnai Spirit microscopy (FEI Company, Hillsboro, OR, USA) 120 kV.

The surface area of the Nb₂O₅NP and Nb₂O₅NP-APS was measured using the multipoint Brunauer-Emmett-Teller (BET) method using a Quantachrome Nova Model 1200E coupled with an automatic nitrogen gas adsorption instrument (Boynton Beach, FL, USA).

The particle size distribution and the nanomaterials stabilities as a function of time were measured by dynamic light scattering (DLS) using a Nanozeta-sizer ZEN 3600 equipment (Malvern, UK) at 633 nm. The zeta potential was determined by laser Doppler electrophoresis also using the Nanozeta-sizer ZEN 3600 equipment. Measurements were made by diluting the suspensions (until 10⁻² mol L⁻¹) in deionized water.

The CHN elemental composition of the Nb₂O₅NP-APS, Nb₂O₅NP-APS-PPIX, and Nb₂O₅NP-APS-PyPh₃ was evaluated using an Elemental Analyzer (PerkinElmer 2400 series II, Shelton, CT, USA). This measurement was done in triplicate and allowed the quantification of the respective dyes.

UV-Vis diffuse reflectance spectra were obtained with a UV-2450 Shimadzu (Kyoto, Japan) spectrometer with

barium sulfate as standard. Samples were scanned from 700 to 250 nm using 1 mm thickness quartz cells.

The infrared (IR) analyses were made using a Nicolet Magna-IR 760 spectrophotometer (Thermo Fisher Scientific, Waltham, MA, USA) (4 cm⁻¹ resolution) and ranging from 4000 to 400 cm⁻¹. All samples were analyzed in KBr pellets at room temperature.

Singlet oxygen (¹O₂) formation was evaluated by following its phosphorescence signal at 1270 nm. Experiments were carried out in an FL900 spectrofluorometer from Edinburgh Instruments (Livingston, UK), coupled with an NIR PMT from Hamamatsu Model H10330-45. All measurements were done in the solid state using the front face geometry. The quantum yield of singlet oxygen formation (Φ_{Δ}) was evaluated by direct comparison of the respective intensities of the phosphorescence emission spectra using phenalenone ($\Phi_{\Delta} = 1.0$, in CCl₄) as standard. Samples were excited at 445 nm and the singlet oxygen emission spectra were obtained from 1240 to 1300 nm. The analysis was carried out using front face configuration on a quartz support. The Φ_{Δ} was calculated, via indirect measurement through the relationship:

$$\Phi_{\Delta NP} = (A_{NP} \times \Phi_{\Delta st}) / A_{st} \quad (1)$$

where $\Phi_{\Delta NP}$ is the singlet oxygen quantum yield for the nanomaterial; A_{NP} is the singlet oxygen emission spectrum area for the nanoparticle; $\Phi_{\Delta st}$ singlet oxygen quantum yield for standard (1.0 in CCl₄); and A_{st} is the singlet oxygen emission spectrum area for the standard (phenalenone).

X-ray photoelectron spectroscopy (XPS) evaluated the chemical composition of the surfaces of the composites. The samples were deposited on carbon sticky paper to avoid surface charging during the analysis. A uniform layer of the samples was placed in an ultrahigh vacuum chamber. The equipment used to perform XPS was an ESCALAB 250Xi spectrometer (Thermo Fisher Scientific, Waltham, MA, USA) equipped with a hemispherical electron energy analyzer. The XPS spectra were collected using a monochromatic Al K α X-ray source with an incident energy = 1486.6 eV. The electron emission angle was 90° with the surface. Survey scans were recorded with 1 eV step and 100 eV analyzer pass energy and the high-resolution regions with 0.1 eV step and 25 eV analyzer pass energy. The linearity of the energy scale was checked using Au 4f line (84.0 eV). Data treatment was performed using the Advantage software (Thermo Fisher) and the C–H signal was used as a reference peak at 284.8 eV binding energy. Peak fitting was carried out with a Lorentzian/Gaussian ratio of 30%/70%.

Cell culture

For PDT experiments, the human lung adenocarcinoma cell line (A549) was employed to assess the potential toxicity of exposure to free dyes and their nano derivatives. The cells were cultured in Dulbecco's Modified Eagle's medium (DMEM) supplemented with 10% fetal bovine serum (FBS), 2 mmol L⁻¹ L-glutamine, 100 U mL⁻¹ penicillin and 100 μ g mL⁻¹ streptomycin (Invitrogen, Carlsbad, CA, USA) at 37 °C in a 5% CO₂ humidified atmosphere.

PDT conditions

Initially, cells (1.25 × 10⁴ cells mL⁻¹) were inoculated in DMEM in a 96-well microplate. After 24 h of growth at 37 °C (in a 5% CO₂ humidified atmosphere), the adherent cells were washed and resuspended in phosphate-buffered saline (PBS) (0.2 M, pH 7.4). Then, cells were exposed to increasing concentrations (5, 10, 15, 20, 30, and 40 μ mol L⁻¹) of the free dyes and the respective immobilized nanomaterials (Nb₂O₅NP-APS-dye) for 1 h. The nanomaterial incubated cells were washed with PBS to remove the excess of non-absorbed nanoparticles before the PDT experiment. The cells were irradiated for 15 min using a light emitting diode (LED, 1.6 J cm⁻²) at the respective maximum of the dyes (PPIX 632 nm, and PyPh₃ 450 nm). The cells that were incubated in PBS without nanoparticles under irradiation were used as controls. After irradiation, the cells were washed twice with PBS, transferred to a drug-free DMEM medium, and allowed to recover for 24 h.²³⁻²⁷

MTT assay

Cell survival was evaluated by the MTT (3-(4,5-dimethylthiazol-2-yl)-2,5-diphenyltetrazolium bromide) mitochondrial-dependent reduction to formazan.²⁶ Cells (1.25 × 10⁴ cells mL⁻¹) in 96 well plates were incubated in DMEM with 10% FBS for 24 h at 37 °C in a 5% CO₂-humidified atmosphere. After this period, cells treated or not with free dyes and their nano-derived materials (Nb₂O₅NP-APS-dye) were subjected to PDT conditions for 15 min and then, re-incubated for 24 h at 37 °C in a 5% CO₂-humidified atmosphere to cell recovery. Before MTT assay the nanomaterials were removed by aspiration and 100 μ L of MTT (0.5 mg mL⁻¹) in DMEM FBS-free was added to the cells. The plates were incubated for 3 h at 37 °C in a 5% CO₂-humidified atmosphere. Then, the MTT was removed from plates by aspiration and the purple formazan crystals were solubilized in DMSO (100 μ L). The extent of reduction of MTT was measured spectrophotometrically

at 570 nm using a microplate reader and directly related to cell viability. Half maximal inhibitory concentration (IC₅₀) was determined by a non-linear regression from the log transformation of the dose-response curves. Results were obtained from at least three independent experiments. All solutions containing dye and nanoparticles were prepared with a 50 millimolar concentration based on CHN analysis. Four balloons were used, each corresponding to a different nanomaterial immobilized, and two additional balloons were used for blank tests one with water and the other with isolated nanoparticles. The various concentrations (5, 10, 15, 20, 30, 40 μmol L⁻¹) were prepared in PBS based on a 50 mmol L⁻¹ stock solution.

Results and Discussion

Nanomaterials must possess special characteristics to work as a PDT agent, probably the capacity to disperse in water and stability under appropriate irradiation are the most important features. These prerequisites can be found when specific dyes are bonded to an oxide like Nb₂O₅. In such scenarios, the nanoparticulate oxide disperses the photosensitizer, reducing molecular aggregation but, also, facilitating cellular endo and exocytosis. To accomplish this, two new structures are proposed and depicted in Scheme 1. As can be seen, a covalent amide bond attaches the Nb₂O₅ to the dyes using APTES as a linker.

The prepared Nb₂O₅NP was initially analyzed by electron microscopy and used to assess the size and structure of the particles. From the SEM image (Figure 1), the particles show a cubic shape with size distribution presenting the main maximum at 120 nm.

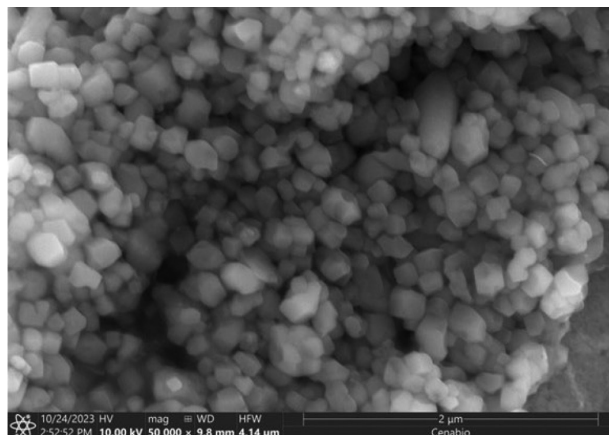
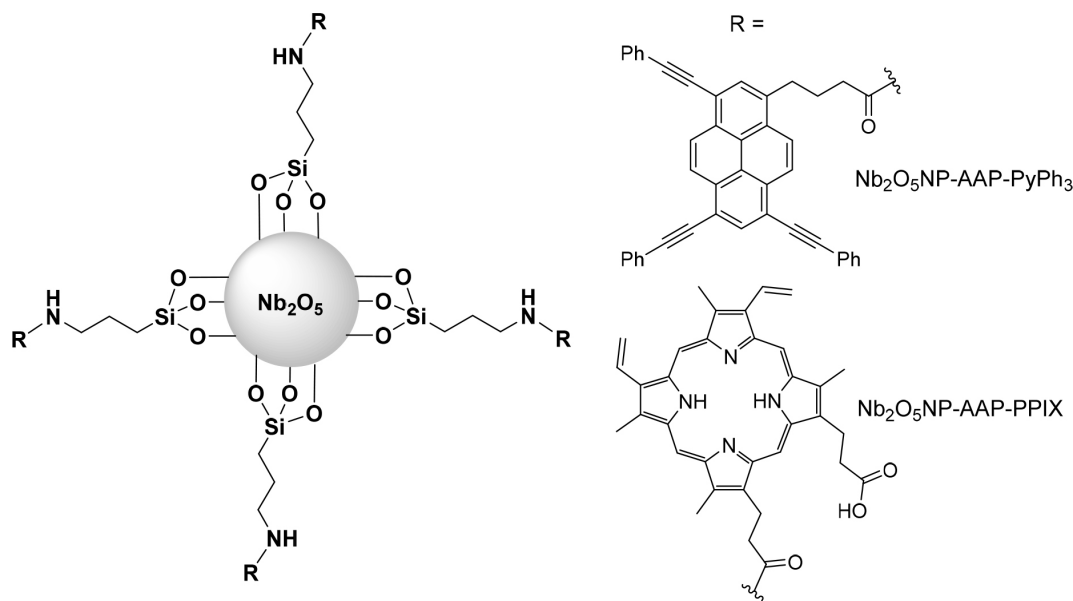


Figure 1. SEM image for Nb₂O₅NP.

The surface area of Nb₂O₅NP obtained by the BET method was 270 m² g⁻¹, which is comparable to other catalysts like TiO₂, ZnO, graphene, and zeolites. The average particle size varies from 120-150 nm. The zeta potential for the Nb₂O₅ nanomaterial is -9.4 mV (in water, pH = 6.5) and -14.8 mV for both dye-modified nanomaterials, indicating lower stabilization when Nb₂O₅ nanomaterial is dye-modified. The lower stabilization for the dye-modified counterparts leads to aggregation after 60 min in deionized water, where the aggregates average size reached 1267 nm. There is no effective difference between Nb₂O₅ nanomaterial and its dye-modified counterparts, indicating low stabilization in all cases.

According to CHN elemental analysis, for Nb₂O₅NP-APS-PPIX was found 0.05 mmol g⁻¹ of the immobilized dye on the nanoparticle surface, while for Nb₂O₅NP-APS-PyPh₃ was 0.31 mmol g⁻¹. The CHN results



Scheme 1. Schematic representation for Nb₂O₅NP-APS-PyPh₃, and Nb₂O₅NP-APS-PPIX.

show that the Nb₂O₅NP surface can be easily decorated with different photosensitizers by the chosen method, which is an important parameter for PDT once it allows for minimizing the amount of administrated photosensitizer.

Diffuse reflectance UV-Vis spectra (Figure 2) show the expected Nb₂O₅NP-APS-PyPh₃ bands at 315 and 413 nm, while 400, 510, 546, 580, and 635 nm for Nb₂O₅NP-APS-PPIX. Both anchored dyes are bathochromically shifted to the respective free dyes in acetonitrile solutions due to the acidic nature of the Nb₂O₅NP surface. Also, the band structure for both dyes agrees with the respective solution patterns.

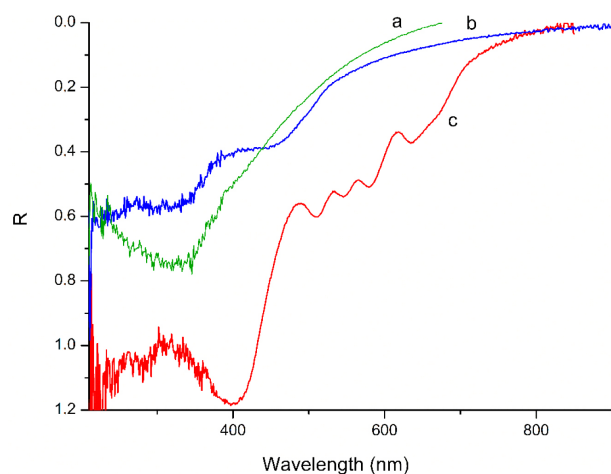


Figure 2. Diffuse reflectance UV-Vis spectra: (a) Nb₂O₅, (b) Nb₂O₅-APS-PyPh₃, and (c) Nb₂O₅-APS-PPIX.

The chemical composition of Nb₂O₅-APS-PPIX, Nb₂O₅-APS-PyPh₃, and Nb₂O₅NP samples was analyzed by the XPS technique. The Nb₂O₅NP sample was used as a reference for Nb binding energy peaks. Survey XPS spectra of the samples are shown in Figure 3a and high-resolution spectra can be found in Figures 3b-3d. As expected, the Nb₂O₅-APS-PPIX and Nb₂O₅-APS-PyPh₃ survey spectra exhibit characteristic silicon emission peaks (Si 2s and Si 2p, with energies around 152 eV and 102.8 eV, respectively) which are absent in the Nb₂O₅NP spectrum. The binding energy of Nb 3d peak in the Nb₂O₅ sample is 207 eV and for Nb₂O₅-APS-PPIX and Nb₂O₅-APS-PyPh₃ samples is 198 eV. The energy shift of the Nb peak is attributed to the surface bond of the Nb–O–Si group in these composites. The presence of Cl peak is due to the residue of thionyl chloride used for composite synthesis.

The high-resolution O1s XPS analysis for the O1s Nb₂O₅ is typical for this oxide according to the literature.²⁸ Otherwise, the Nb₂O₅-APS-PPIX and Nb₂O₅-APS-PyPh₃ samples present three main components: O–Nb, O–Si, and a carboxyl feature with binding energies centered at 530, 531.9, and 533.8 eV, respectively. Over again, the

presence of the Si–O peak for the Nb₂O₅-APS-PyPh₃ sample confirms the synthesized structure.

Singlet oxygen formation

As a possible photosensitizer candidate, the material must absorb light and follow a cascade of events culminating with the energy transfer to triplet oxygen singlet dissolved in the cell medium, as in Scheme 2.

Scheme 2 shows that the dyes follow a complex cascade of events that can eventually generate singlet oxygen if the dye in the triplet state succeeds in encountering a triplet molecular oxygen. So, as can be seen, PDT is intrinsically dependent upon the formation of singlet oxygen. Fortunately, this species is a phosphorescent transient whose detection is made at 1270 nm. So, the phosphorescence of both materials Nb₂O₅-APS-PPIX and Nb₂O₅-APS-PyPh₃ (pellets) were analyzed following the excitation of the respective dyes and Figure 4 shows the singlet oxygen phosphorescence at 1270 nm in the solid state. The obtained phosphorescence signals were also used to evaluate the singlet oxygen quantum yield for both Nb₂O₅NP-APS-PPIX and, Nb₂O₅NP-APS-PyPh₃. By using the direct correlations as equation 1, the quantum yields are 0.65 and 0.77, respectively. It is worthwhile to note that the free PPIX shows a singlet oxygen quantum yield of 0.50 and PyPh₃ is 0.40 (in CCl₄).²⁰ As can be seen, the nanoparticles provide an ambient capable of preventing aggregation and, consequently, avoiding significant excited state deactivation, thus, facilitating the crossing to the triplet state and consequently, the singlet oxygen formation. Both materials show no phosphorescence emission when the sample is deoxygenated with Ar.

Cell damage induced by singlet oxygen sensitized by Nb₂O₅-APS-PPIX and Nb₂O₅-APS-PyPh₃ nanoparticles

As a preliminary result, it is worthwhile to note that no cell damage was detected in dark conditions (data not shown). These results corroborate with data from the literature in terms of the absence of cytotoxicity in the dark. Otherwise, according to Scheme 2, once nanomaterials Nb₂O₅-APS-PyPh₃ and Nb₂O₅-APS-PPIX were irradiated, the excited dyes followed a photochemical cascade that culminated with singlet oxygen formation (Figure 4), which triggered the cell damage process. As Figure 5 shows, ca. 65% of cell survival is found when the pristine Nb₂O₅ nanoparticles are used. This result is likely attributed to the formation of other ROS like superoxide anion radical, hydroxyl radical, and hydroperoxyl radical. Also, for low concentrations, the cytotoxicity of nanomaterials is lower

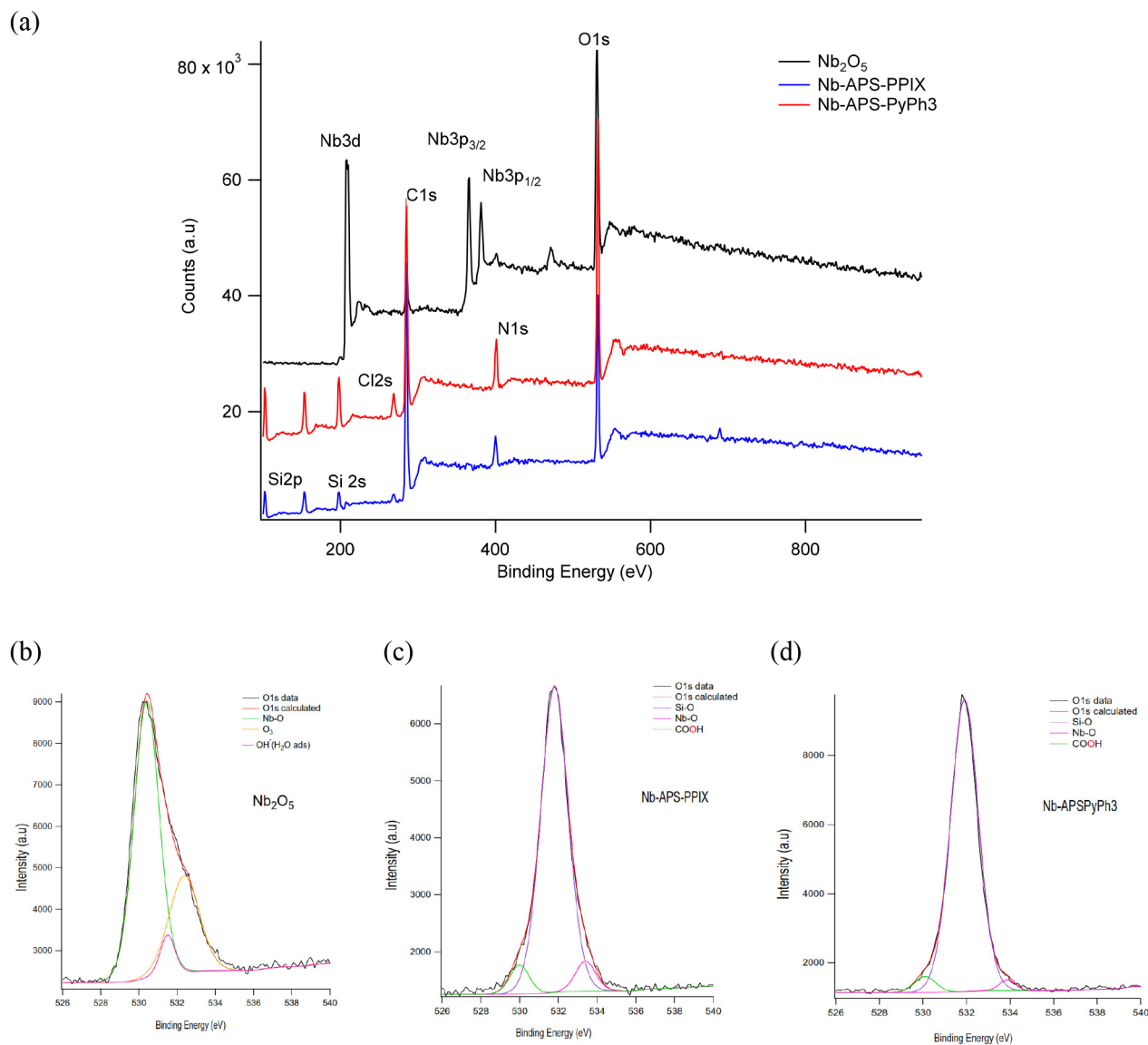
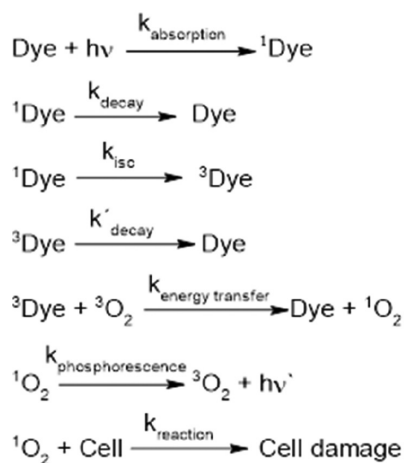


Figure 3. XPS analysis survey spectra (a) and XPS signal deconvolution for Nb₂O₅NP (b), Nb₂O₅-APS-PPIX (c) and, Nb₂O₅-APS-PyPh₃ (d).



Scheme 2. Photochemical paths for the dye in excited states; k_{decay} is related to all excited state deactivation possibilities.

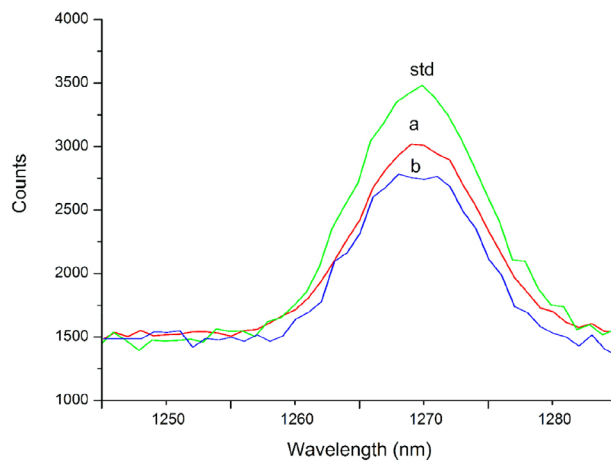


Figure 4. Singlet oxygen emission: (std) standard phenalenone; (a) Nb₂O₅NP-APS-PyPh₃ and (b) Nb₂O₅NP-APS-PPIX.

than that for the respective free dyes. At the concentration of 5 $\mu\text{mol L}^{-1}$ the survival rate for the free PyPh₃ dye was approximately 50%, while for the Nb₂O₅-APS-PyPh₃ nano drug derivative, the survival reached approximately 70% (Figure 5a). As observed for PyPh₃ and its nano-drug derivative, the free PPIX dye phototoxicity, at the same concentration, was ca. 50%, while for the Nb-APS-PPIX nano-drug, a 70% survival was observed (Figure 5b). As expected, exposing cells to higher concentrations of free dyes led to an increase in cell susceptibility. The exposure of cells to increasing concentrations of nanomaterial also affected cell survival; however, the reduction was less pronounced. When photosensitizers were employed at 40 $\mu\text{mol L}^{-1}$, the free PyPh₃ dye showed a 20% survival, while for the Nb-APS-PyPh₃ this value dropped to about 20%. Similarly, for the free PPIX dye (at 40 $\mu\text{mol L}^{-1}$), the survival rate was approximately 20%, while for its Nb₂O₅-APS-PPIX nano-drug, it was less than 30%. It is possible to note that, for higher concentrations, the survival viability of the A549 cells drops significantly after 15 min of photoexcitation. Furthermore, A549 cells treated with PPIX and PyPh₃ presented IC₅₀ values of 4.7 ± 0.06 and 5.4 ± 0.04 $\mu\text{mol L}^{-1}$, respectively. In contrast, the IC₅₀ for Nb₂O₅-APS-PPIX and Nb₂O₅-APS-PyPh₃ was 13.1 ± 0.02 and 11.9 ± 0.02 $\mu\text{mol L}^{-1}$, respectively. Herein, our results follow the literature on phototoxicity assays for different types of nanomaterial containing the PPIX dye and a previous study on the PyPh₃ compound.²⁰

In general, the present study recapitulates data from the literature concerning increased phototoxicity with nano drug concentration. In the case of PyPh₃ it is also important to note that in a previous study,²⁰ we showed that this dye is a promising PS for application in PDT due to a high antitumor photoactivity (IC₅₀ 6.5 $\mu\text{mol L}^{-1}$) and the absence of toxicity in the *Galleria mellonella* model of study at higher concentration (70.0 mmol L^{-1}).

Conclusions

In this paper, PPIX and PyPh₃ covalently linked to Nb₂O₅ nanoparticles were prepared and successfully tested in A549 tumor cell line as new promising PDT materials. The *in vitro* study showed IC₅₀ ca. 12 $\mu\text{mol L}^{-1}$ for both materials and the absence of dark conditions. In conclusion, while the evaluated materials are promising, it is essential to note that such an assertion may be premature. Further comprehensive evaluations are imperative, encompassing additional *in vitro* parameters such as activation of cell apoptosis, inhibition of invasiveness, cytotoxicity in non-tumor cells, and the determination of the selectivity index. Additionally, an assessment of experimental animal toxicity, along with the evaluation of pharmacokinetic parameters, is crucial before considering these materials as viable candidates for preclinical studies. A thorough investigation of these aspects will provide a more comprehensive understanding of the suitability of the material and safety profile, paving the way for informed decisions in advancing towards clinical applications.

Acknowledgments

The authors thank the Conselho Nacional de Desenvolvimento Científico e Tecnológico (CNPq), Coordenação de Aperfeiçoamento de Pessoal de Nível Superior (CAPES), Fundação Carlos Chagas Filho de Amparo à Pesquisa do Estado do Rio de Janeiro (FAPERJ) for their financial support and fellowships and Instituto Nacional de Tecnologias Alternativas para Detecção, Avaliação Toxicológica e Remoção de Micropoluentes e Radioativos (INCT-DATREM).

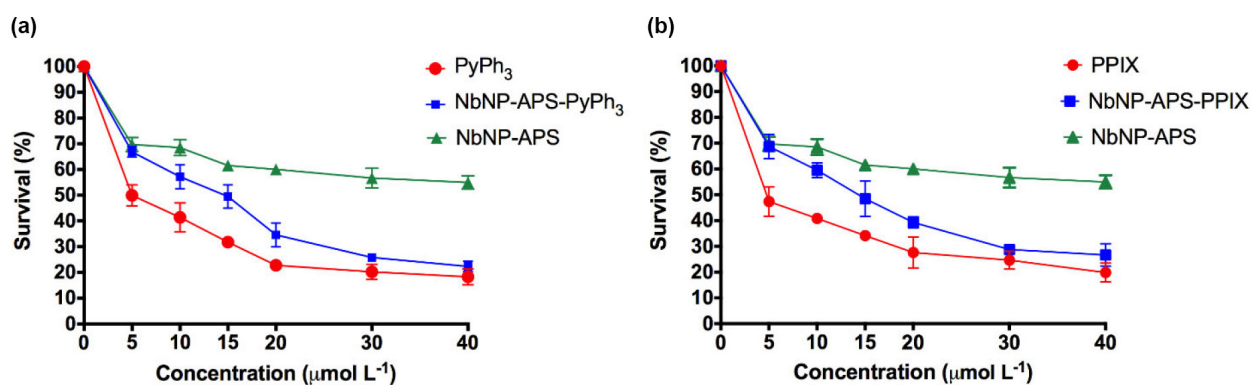


Figure 5. PDT effect on the cytotoxicity of the A549 tumor cell line after treatment with (a) Nb₂O₅NP-APS-PPIX and (b) Nb₂O₅NP-APS-PyPh₃. Cells were subjected to PDT (15 min) in PBS after incubation with photo drugs. Cell survival was determined by MTT assay after 24 h of cell recovery in DMEM. Results are mean \pm standard deviation of three independent experiments ($*p < 0.0001$ compared to control (Nb₂O₅NP-APS)). All statistics were performed by two-way analysis of variance (ANOVA) using Dunnett.

Author Contributions

R.C.S.O., L.C., Z.G. were responsible for conceptualization, data curation, validation, visualization, and writing-review; M.D.P., J.S.B.F., G.S., E.S.R., R.J.C. for writing original draft, investigation, writing-review, resources, and editing.

References

1. Ferlay, J.; Shin, H.-R.; Bray, F.; Forman, D.; Mathers, C.; Parkin, C. M.; *Int. J. Cancer* **2010**, *127*, 2893. [Crossref]
2. Guo, Y. Y.; Rogelj, S.; Zhang, P.; *Nanotechnology* **2010**, *21*, 065102. [Crossref]
3. Jia, X.; Jia, L.; *Curr. Drug Metab.* **2012**, *13*, 1119. [Crossref]
4. Alexis, F.; Rhee, J. W.; Richie, J. P.; Radovic-Moreno, A. F.; Langer, R.; Farokhzad, O. C.; *Urol. Oncol.: Semin. Orig. Invest.* **2008**, *26*, 74. [Crossref]
5. DeRosa, M. C.; Crutchley, R. J.; *Coord. Chem. Rev.* **2002**, *233*, 351. [Crossref]
6. Peres, M. F. S.; Nigoghossian, K.; Primo, F. L.; Saska, S.; Capote, T. S. O.; Caminaga, R. M. S.; Messaddeq, Y.; Ribeiro, S. J. L.; Tedesco, A. C.; *J. Braz. Chem. Soc.* **2016**, *27*, 1949. [Crossref]
7. Dąbrowski, J. M.; *Adv. Inorg. Chem.* **2017**, *70*, 343. [Crossref]
8. Robertson, C. A.; Evans, D. H.; Abrahamse, H.; *J. Photochem. Photobiol., B* **2009**, *96*, 1 [Crossref]; Chen, L.; Huang, J.; Li, X.; Huang, M.; Zeng, S.; Zheng, J.; Peng, S.; Li, S.; *Front. Bioeng. Biotechnol.* **2022**, *31*, 920162. [Crossref]
9. Swarnalatha, S.; Khee, L.; Chee, S.; Yong, Z.; *Chem. Rev.* **2015**, *115*, 1990. [Crossref]
10. Arias-Egido, E.; Laguna-Marco, M. A.; Piquer, C.; Jiménez-Cavero, P.; Lucas, I.; Morellón, L.; G.; Gallego, F.; Rivera-Calzada, A.; Cabero-Piris, M.; Santamaria, J.; Fabbris, G.; Haskel, D.; Boada, R.; Díaz-Moreno, S.; *Nanoscale* **2021**, *13*, 17125. [Crossref]
11. Duo, Y.; Luo, G.; Li, Z.; Chen, Z.; Li, X.; Jiang, Z.; Yu, B.; Sun, Z.; Yu, X.-F.; *Small* **2021**, *17*, 2103239. [Crossref]
12. Guo, X.; Wen, C.; Xu, Q.; Ruan, C.; Shen, X.-C.; Liang, H.; *J. Mat. Chem. B* **2021**, *9*, 2042. [Crossref]
13. Younis, M. R.; He, G.; Qu, J.; Lin, J.; Huang, P.; Xia, X. H.; *Adv. Sci.* **2021**, *8*, 2102587. [Crossref]
14. Yu, S.; Zhou, Y.; Sun, Y.; Wu, S.; Xu, T.; Chang, Y.-C.; Bi, S.; Jiang, L.-P.; Zhu, J.-J.; *Angew. Chem., Int. Ed.* **2021**, *60*, 5948. [Crossref]
15. Yuan, X.; Cen, J.; Chen, X.; Jia, Z.; Zhu, X.; Huang, Y.; Yuan, G.; Liu, J.; *J. Colloid Interface Sci.* **2022**, *605*, 851. [Crossref]
16. Nakajima, K.; Fukui, T.; Kato, H.; Kitano, Kondo, J. N.; Hayashi, S.; Hara, M.; *Chem. Mater.* **2010**, *22*, 3332. [Crossref]
17. Furukawa, S.; Ohno, Y.; Shishido, T.; Teramura, K.; Tanaka, T.; *J. Phys. Chem. C* **2013**, *117*, 442. [Crossref]
18. Ziolec, M.; *Catal. Today* **2003**, *78*, 47. [Crossref]
19. Prado, A. G. S.; Bolzon, L. B.; Pedroso, C. P.; Moura, A. O.; Costa, L. L.; *Appl. Catal., B* **2008**, *82*, 219. [Crossref]
20. de França, B. M.; Forero, J. S. B.; Garden, S. J.; Ribeiro, E. S.; Souza, R. S.; Teixeira, R. S.; Corrêa, R. J.; *Dyes Pigm.* **2018**, *148*, 444. [Crossref]
21. Uekawa, N.; Kudo, T.; Mori, F.; Wu, Y. J.; Kakegawa K.; *J. Colloid Interface Sci.* **2003**, *264*, 378. [Crossref]
22. Oliveira, R. C.; Corrêa, R. J.; Teixeira, R. S.; Queiroz, D. D.; Souza, R. S.; Garden, S. J.; de Lucas, N. C.; Pereira, M. D.; Forero, J. S. B.; Romani, E. C.; Ribeiro, E. S.; *J. Photochem. Photobiol., B* **2016**, *165*, 1. [Crossref]
23. da Silva, D. B.; da Silva, C. L.; Davanzo, N. N.; Souza, R. S.; Corrêa, R. J.; Tedesco, A. C.; Pierre, M. B. R.; *Photodiagn. Photodyn. Ther.* **2021**, *35*, 102317. [Crossref]
24. Miguel, J. O.; da Silva, D. B.; da Silva, G. C. C.; Corrêa, R. J.; Miguel, N. C. O.; Lione, V. O. F.; Pierre, M. B. R. *J. Photochem. Photobiol., A* **2020**, *386*, 112109. [Crossref]
25. Denizot, F.; Lang, R.; *J. Immunol. Methods* **1986**, *89*, 271. [Crossref]
26. Senaratne, S. G.; Pirianov, G.; Mansi, J. L.; Arnett, T. R.; Colston, K. W.; *Br. J. Cancer* **2000**, *82*, 1459. [Crossref]
27. Sieuwerts, A. M.; Klijn, J. G. M.; Peters, H. A.; Foekens, J. A.; *Eur. J. Clin. Chem. Clin. Biochem.* **1995**, *33*, 813. [Crossref]
28. Weibin, Z.; Weidong, W.; Xueming, W.; Xinlu, C.; Dawei, Y.; Changle, S.; Liping, P.; Yuying, W.; Li, B.; *Surf. Interfaces Anal.* **2013**, *45*, 1206. [Crossref]

Submitted: December 7, 2023

Published online: March 19, 2024